Irreversibility line in superconducting $HgBa_2CuO_{4+\delta}$ single crystals

M. Pissas, E. Moraitakis, G. Kallias, A. Terzis, and D. Niarchos
Institute of Materials Science, NCSR Demokritos, 15310 Ag. Paraskevi, Athens, Greece

M. Charalambous
Centre de Recherches sur les Tres Basses Temperatures, CNRS, BP166X, 38042 Grenoble, France
(Received 10 February 1998)

The vortex phase diagram in $HgBa_2CuO_{4+\delta}$ single crystals ($T_c=95$ K) is investigated using dc-magnetic measurements. The irreversibility magnetic field $H_{irr}(T)$ decreases exponentially in the temperature range $20\leqslant T\leqslant 88$ K. At $T^*\approx 88$ K, the $H_{irr}(T)$ curve changes slope abruptly and a new mechanism controls the irreversibility up to T_c. Magnetization versus magnetic field measurements ($\mathbf{H}\|c$) show a second peak (increase of the critical current) in the range $5\leqslant T\leqslant 50$ K. The overall picture resembles the phase diagram of the $Bi_2Sr_2CaCu_2O_{8+\delta}$ and $YBa_2Cu_3O_7$ compounds if one considers the anisotropy $\varepsilon=(m/M)^{1/2}$ of $HgBa_2CuO_{4+\delta}$, which lies in between the two others. [S0163-1829(98)00938-2]

I. INTRODUCTION

The simplicity of the structure, the high symmetry, the relatively high superconducting transition temperature, and the possibility for variation of the oxygen content from the underdoped to the overdoped regime of the $n=1$ member of the mercury-based family of cuprates $[HgBa_2Ca_{n-1}Cu_nO_{2n+2+\delta}]$ make it an excellent reference compound for physical properties measurements. The first step for a serious study of $HgBa_2CuO_{4+\delta}$ (Hg-1201) is the growth of high quality single crystals. Hg-1201 decomposes at ambient pressure before melting and the volatile components evaporate, whereas for $P(O_2)\approx 21.3$ kPa the decomposition temperature is between 706 and 822 °C and is accompanied by a complete removal of HgO.[1] The only way to prevent decomposition before the sample reaches the peritectic temperature is to use high hydrostatic inert-gas pressure (10^9 Pa).[2] Recently, considerable progress has been done in Hg-1201 single-crystal growth.[3–7]

The structure of Hg-1201 compound (see Fig. 1) consists of a stacking of layers $[HgO_\delta\ BaO\ CuO_2\ BaO\ HgO_\delta]$, where the square brackets include the contents of one unit cell. The extra oxygen, which causes the electrical doping, is located at the (1/2,1/2,0) site of the Hg plane. Copper has a very elongated octahedral coordination with distance between Cu and the apical oxygen $[d(\mathrm{Cu-O(1)})\simeq 2.8$ Å] to be significantly larger than the Cu-O distances $[d(\mathrm{Cu-O(2)})\simeq 1.94$ Å] in planes perpendicular to c axis. Moreover, the compound $HgBa_2CuO_{4+\delta}$ can be considered as stacking of quasi two-dimensional (quasi-2D) CuO planes. The distance of CuO planes is $\simeq 9.5$ Å.

It is generally accepted that high anisotropy plays a primary role in the complexity of the magnetic phase diagram of high-temperature superconductors. The decrease of the anisotropy parameter[8] $\varepsilon[\varepsilon=\sqrt{m/M}\equiv\lambda_{ab}(0)/\lambda_c(0)\equiv\xi_c(0)/\xi_{ab}(0)]$ due to the layered structure enhances the Ginzburg number[8] $Gi\propto T_c^4/\varepsilon^2$ so that the fluctuations become relevant. The cuprate superconductors discovered up to today present a variation of the anisotropy which depends mainly on the crystal structure (distance of Cu-O planes and number of planes in each block). The parameter ε^{-1} for optimally doped $HgBa_2CuO_{4+\delta}$ lies between that of optimally doped $YBa_2Cu_3O_{7-\delta}$ (more 3D, $\varepsilon^{-1}=5$) and $Bi_2Sr_2CaCu_2O_{8+\delta}$ (more 2D, $\varepsilon^{-1}=50$).[9] Consequently, we expect the values of the physical parameters of Hg-1202 to lie between $YBa_2Cu_3O_{7-\delta}$ and $Bi_2Sr_2CaCu_2O_{8+\delta}$.

In this work we report on the crystal structure of as-grown Hg-1201 single crystals and a detailed and complete set of dc-magnetic measurements using a commercial superconducting quantum interference device (SQUID) magnetometer from 5 K up to the transition temperature (T_c) and for magnetic fields 0–50 kOe.

II. EXPERIMENT

The characterization part of the single crystals was performed with a miniaturized GaAsIn Hall sensor with active area $10\times 10\ \mu m^2$. The single crystals were placed on top of the active area of the Hall probe and an ac-magnetic field ($f=3$ Hz, amplitude 0.1–10 Oe) was applied. The real and

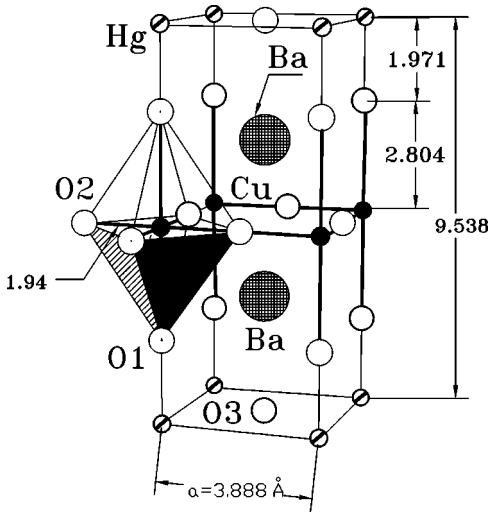

FIG. 1. Crystal structure of the $HgBa_2CuO_{4+\delta}$ compound.

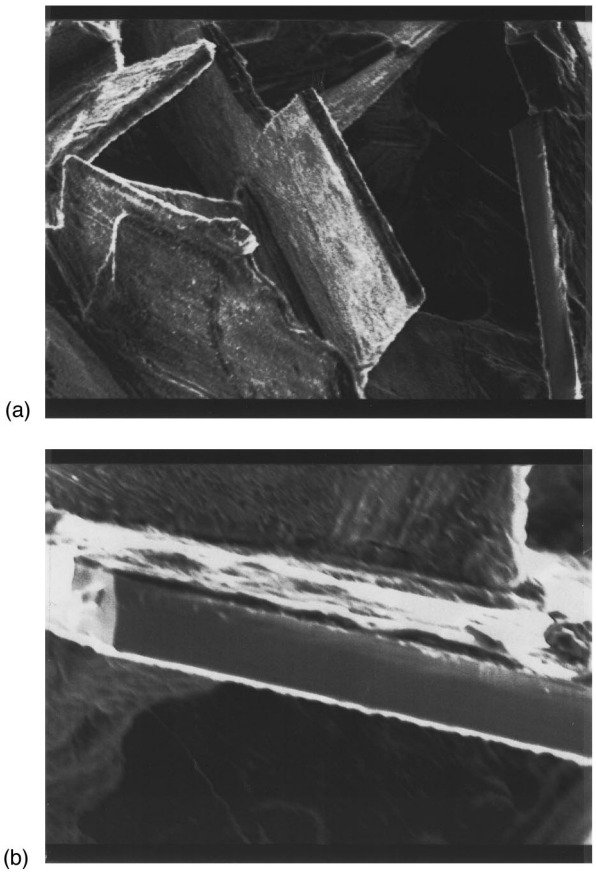

FIG. 2. Scanning electron micrograph of $HgBa_2CuO_{4+\delta}$ single crystals. (a) The arrangement of as-grown crystals inside the cavity. (b) The very flat ac side of a single crystal.

imaginary parts of the Hall voltage were measured by using a lock-in amplifier. The ac resolution attained with this system is $\approx$20 mOe. dc-magnetization measurements were performed in a SQUID magnetometer (Quantum Design).

III. CRYSTAL GROWTH

The single-crystal growth was carried out in sealed silica tube at 1100 °C using an alumina crucible. Since the melting point of the Ba_2CuO_{3+y} compound is near the melting point of Au, Au foil melts frequently and the reaction of Ba_2CuO_{3+y} with the quartz tube leads to explosions. To overcome this difficulty we used dense alumina crucibles instead of Au. The alumina crucible was placed in a temperature gradient of $\sim$10 °C/cm, the bottom being at the higher temperature. Melting was observed and inside the solidified material we found cavities containing the single crystals. Figure 2 shows single crystals in such a cavity. The dimensions of the single crystals were up to $1000\times1000\times30$ μm^3. T_c for the majority of those crystals was around 88 K, but there were also crystals with $T_c=95$ K. Annealing in flowing O_2 at 300–400 °C increases T_c to 95 K. Figure 3 shows the local ac susceptibility for a single crystal as a function of temperature at various stages of the oxygen post-annealing process.

IV. SINGLE-CRYSTAL STRUCTURE DATA

For the diffraction experiments, a single crystal with approximate dimensions $200\times200\times20$ μm^3 was mounted on

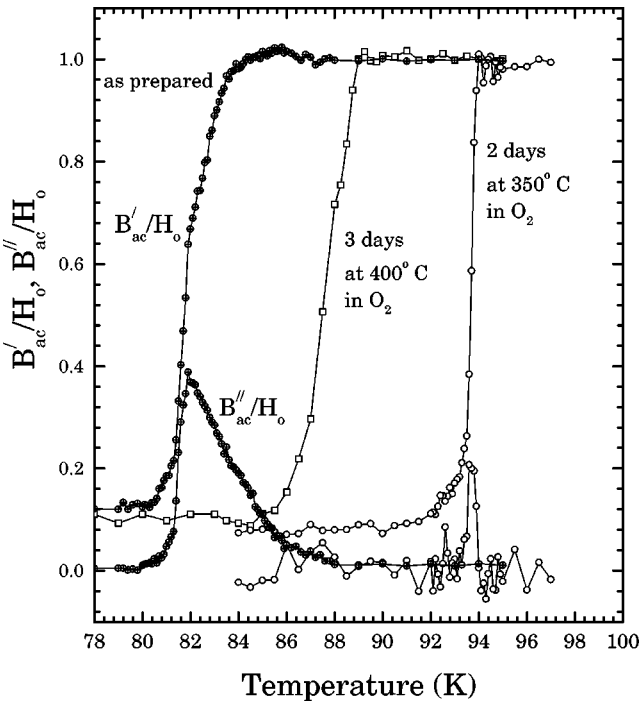

FIG. 3. Local ac susceptibility for a Hg-1201 single crystal as prepared, annealed in oxygen flow for 3 days at 400 °C followed by 2 days at 350 °C.

a Crystal Logic dual goniometer diffractometer using graphite monochromated Mo radiation. The unit cell dimensions were determined and refined by using angular settings of 25 automatically centered reflections in the range $11°<2\theta<23°$ and they appear in Table I. Intensity data were recorded using a θ-2θ scan to 2θ (max)$=70°$ with scan speed 3.0 deg/min and scan range $2.5°+\alpha_1\alpha_2$ separation. Three standard reflections monitored every 97 reflections showed less than 3% variation and no decay. Lorentz, polarization and ψ-scan absorption corrections were applied using Crystal Logic software. Symmetry equivalent data were averaged with $R=0.059$ to give 225 independent reflections from a total of 2350 collected. The structure was solved by direct methods using SHELXS-86 and refined by full-matrix least-squares techniques of F^2 (with SHELXS-93) using 225 reflections and refining 16 parameters. All atoms were refined anisotropically except for the deficient O(3) atom. The final values for R_1, wR_2, and goodness of fit (GOF) for all data are 0.032, 0.083 and 1.202, respectively. The maximum and minimum residual peaks in the final difference map were 4.02 and -2.93 $e/\text{Å}$. The largest shift/e.s.d. in the final cycle was 0.003. Positional and U thermal parameters are given in Table II and selected bond distances and thermal parameters in Table III.

In the first step we refined only the position of the heavy atoms (Hg, Ba, Cu) with anisotropic displacement factors. At this stage of refinement the reliability factors were $R_1=0.0418$, $wR_2=0.0919$, and GOF$=1.255$. As a second step we refine in addition the positions and anisotropic displacement factors of O(1) and O(2), thereby reducing the reliability factors to $R_1=0.0334$, $wR_2=0.0836$, and GOF$=1.206$. Analysis of difference Fourier maps revealed three peaks. The first was 0.7 Å from Hg atoms, the second 0.6 Å from Ba atoms, and the third was at the (1/2,1/2,0) position. The

TABLE I. Crystal data and experimental conditions for $HgBa_2CuO_{4+\delta}$ single crystals. $W=1/[\sigma^2(F_0^2)+(aP)^2+bP]$, $P=[\mathrm{Max}(F_0^2,0)+2*F_c^2)/3$, $R_1=\Sigma||F_o|-|F_c||/\Sigma|F_o|$, $wR_2=[\Sigma w(F_o^2-F_c^2)^2/\Sigma wF_o^4]^{1/2}$

Wavelength	0.71073
Space group	$P4/mmm$
a (Å)	3.888(1)
c (Å)	9.538(3)
V (Å^3)	144.211
ρ (g cm^{-3})	6.941
Abs. coefficient (μ) (cm^{-1})	435.5
Scan mode/speed (deg/min)	$\theta-2\theta/3$
Scan range (deg)	$2.5^0+\alpha_1\alpha_2$ separation
2θ range (deg)	2 to 68
Min (abs. correction factor)	1.02
Max (abs. correction factor)	19.20
Range of h,k,l	$-6\leqslant h\leqslant 6,-6\leqslant k\leqslant 6,-15\leqslant l\leqslant 15$
W	$\alpha=0.0523,\ b=0.72$
$\Delta\rho_{max}/\Delta\rho_{min}$ (e/Å^3)	4.02/−2.93
Refinement method	Full matrix least squares on F^2
Data/restraints/parameters	225/0/16
Goodness of fit on F^2	1.206
Final R indices $224>4\sigma(I)$	$R_1=0.0326,\quad wR_2=0.0547$
R indices (all data)	$R_1=0.0329,\quad wR_2=0.0827$

peaks near Hg and Ba come from truncation errors. The third peak corresponds to the oxygen-deficient site (1/2,1/2,0). Referring to the peak at (1/2,1/2,0), it obviously corresponds to extra oxygen within the mercury plane. Keeping the isotropic displacement factor constant at 0.012, which is the average value of O(1) and O(2), we refined the oxygen occupancy for this site. The estimated value for the extra oxygen was 8 ± 4 %, while the reliability factors were further reduced.

The structure of the Hg-1201 compound is shown schematically in Fig. 1. It possesses a lamellar structure similar to all the cuprate superconductors, which is infinitely extended along the a and b crystallographic directions. The stacking of the layers along the c axis is [HgO_δ BaO CuO_2 BaO HgO_δ], where the square brackets include the contents of one unit cell.

Copper has a very elongated octahedral coordination with the distance between Cu and the apical oxygen [d(Cu−O(1))≃2.8 Å] significantly larger than the Cu-O distances in the ab-plane [d(Cu−O(2))≃1.94 Å]. As a result its coordination can be consider as quasi-square planar. The CuO layers stack along the c axis and are separated by two BaO_2 and one HgO_δ layers, so that the distance of consecutive CuO planes along the c axis is ≃9.5 Å. The thermal ellipsoids of Cu, Ba, and O(2) (plane oxygen) ions are strongly anisotropic along the c axis with $U_{33}\approx g\times U_{11}$ ($g=2-3$), contrary to the mercury and O(1) (apical oxygen) ions for which the thermal ellipsoids are nearly isotropic.

The extra oxygen (≃8%) that causes the electrical doping is located at the ($\frac{1}{2},\frac{1}{2}$,0) site in the Hg plane. The determination of small oxygen concentrations ⩽20% in the vicinity of such a heavy scatterer as Hg from x-ray data is a difficult problem and the correct solution depends on many factors, e.g., the choice of structural model or algorithm for the absorption correction. The quality of the diffraction experiment is related to the statistics and the diffractometer resolution is also very important.

An extensive discussion of the crystal structure determination from powder samples using x-ray and neutron data and the associated problems is given in Refs. 7 and 10–13 The crystal structure parameters from powder and single-crystal data are in principle the same. Our crystal structure data are in agreement with those of Ref. 4, except for a small difference of 0.03 Å in the c-axis length for the same T_c. The anisotropic thermal displacement factors can be considered to be practically the same. It is worth mentioning that the estimated oxygen content is also very close to their value. Our data are comparable with those of Pelloquin *et al.*;[6] e.g., there is perfect agreement in the cell constants, although a direct comparison is impeded by their complicated structural model. Finally, our results are also in agreement with those of Bordet *et al.*[5] (model 1), where they discuss several structural models based on the possible substitution of CO_3^{-2} in the Hg sites.

V. MAGNETIC MEASUREMENTS

First, we present our experimental results for the magnetic moment vs temperature variation at low dc magnetic fields.

TABLE II. Fractional atomic coordinates, anisotropic and equivalent isotropic thermal displacement factors U_{ij}, U_{eq} (in Å^2), and occupancy factors for a $HgBa_2CuO_{4+\delta}$ single crystal with $T_c=95$ K and cell constants $a=3.888(1)$ Å and $c=9.538(3)$ Å. The anisotropic displacement thermal factor exponent takes the form $-2\pi^2[h^2a^{*2}U_{11}+\cdots+2hka^*b^*U_{12}]$. Numbers in parentheses are statistical errors of the last significant digit.

Atom	WN	x	y	z	U_{11}	U_{33}	U_{eq}	N
Hg	1a	0	0	0	0.0163(3)	0.0118(3)	0.0148(3)	1.0
Ba	2h	$\frac{1}{2}$	$\frac{1}{2}$	0.2995(1)	0.0062(2)	0.0118(3)	0.0081(3)	1.0
Cu	1b	0	0	$\frac{1}{2}$	0.0030(5)	0.0114(7)	0.0058(4)	1.0
O(1)	4g	0	0	0.2066(9)	0.018(2)	0.014(4)	0.017(1)	1.0
O(2)	2e	0	$\frac{1}{2}$	$\frac{1}{2}$	0.005(2)[a]	0.018(3)	0.008(1)	1.0
O(3)	1c	$\frac{1}{2}$	$\frac{1}{2}$	0	-	-	0.012	0.08(4)

[a] $U_{22}=0.001(2)$.

TABLE III. Interatomic distances (Å) from the structure data of a $HgBa_2CuO_{4+\delta}$ single crystal with $T_c = 95$ K.

Hg-O(1)	× 2	1.971(9)
Hg-O(3)	× 4	2.749(1)
Ba-O(1)	× 4	2.889(3)
Ba-O(2)	× 4	2.727(1)
Ba-O(3)	× 1	2.857(1)
Cu-O(1)	× 2	2.798(3)
Cu-O(2)	×4	1.944

Figure 4(a) shows the variation of the magnetic moment with temperature in a constant dc-magnetic field applied nearly parallel to the c axis of the crystal after zero-field cooling (ZFC). For a small dc-magnetic field the magnetic moment is constant and only near T_c does it abruptly go to zero. The onset of the transition for these fields is $T_c \simeq 95 \pm 0.5$ K. The width of the transition for $H_{dc} = 12$ Oe (90%–10%) is about 2 K. Based on the derivative of the magnetic moment with temperature (dm/dT) curve we can define four characteristic points on the $m(T)$ curve. For clarity let us discuss the measurement with $H_{dc} = 390$ Oe using the dm/dT curve [see Fig. 4(b)]. At low temperatures m is nearly constant and at some temperature T_0 a shoulder starts to develop. Above T_0, $m(T)$ is convex up to an inflection point (T_i). Then, as T increases, $m(T)$ becomes concave until temperature T_{sh} and after exceeding T_{sh} it varies approximately linearly with T. At the vicinity of T_c it is curved again. The shoulder is pronounced very clearly for $H_{dc} > 190$ Oe. We note that for $H_{dc} < 350$ Oe and $T > T_{sh}$ the $m(T)$ curve becomes convex again. The three characteristic temperatures move to lower values as the magnetic field increases.

A reasonable explanation of the observed behavior (for $H \leqslant 145$ Oe) could be given using a simple model developed by Clem and Hao.[14] A shoulder like the $m(T)$ shape could arise from the crossing of H_{dc} with $H_{c1}(T)$ (the lower critical field at temperature T) as the temperature increases.[14] For $T < T_{c1}$ the crystal is in the Meissner state, and at T_{c1}, H_{dc} is equal to H_{c1}. Induced currents (which produce the magnetic moment) are flowing within λ of the surface and screen the bulk of the crystal from the applied field ($4\pi M/H_{dc} = -1$). For $T_{c1} \leqslant T \leqslant T_{sh}$ the magnetic flux gradually penetrates into the sample until T_{sh}, where the flux front reaches the middle of the sample. Above T_{sh}, $-m$ decreases due to the decrease of the critical flux gradient (and/or of the critical current). In the temperature range $T_{c1} < T < T_c(H_{dc})$ the specimen is in the mixed state. In the absence of pinning and surface and/or geometrical barriers the flux density B, averaged over the intervortex spacing, is uniform inside the specimen and equal to the reversible flux density in equilibrium with a magnetic field H. When pinning is present the magnetization for $T_{c1} < T < T_c(H_{dc})$ cannot achieve its equilibrium value and pinning forces tend to hold the vortices near the surfaces, building up a critical flux-density gradient. In this model T_{c1} is expected to increase according to the temperature variation of $H_{c1}(T)$ up to the T_c region.[15,16]

The ZFC measurements for $H > 154$ Oe, although showing the shoulder, needs a different explanation. More specifically m for $T < T_0$ is not constant and the temperature where the shoulder starts to develop is roughly confined to a small field window. Our measurements resemble the low-magnetic-field ZFC m vs T data for a $Bi_2Sr_2CaCu_2O_{8+\delta}$ single crystals.[17] In $Bi_2Sr_2CaCu_2O_{8+\delta}$ for $H > 100$ Oe the flux exclusion is dramatically suppressed at a weakly field-dependent temperature around 20 K. After this temperature $-m(T)$ decreases up to the T_c. In other words, the critical current suffers a sudden reduction to rather small values at a temperature well below $T_{irr}(H)$. As De la Cruz *et al.*[17] pointed out the rapid change in the critical current capability indicates a transition from one pinned vortex state to another with much lower critical current. This transition takes place at a temperature that was defined by the shoulder observed in the $m(T)$ curves. Recently, Goffman *et al.*[18] attributed the steep decrease of perpendicular permeability $\mu_\perp$ in single-crystal measurements at 22 K to a large increase in the critical current, associated with the crossover to the zero-dimensional pinning regime.[19]

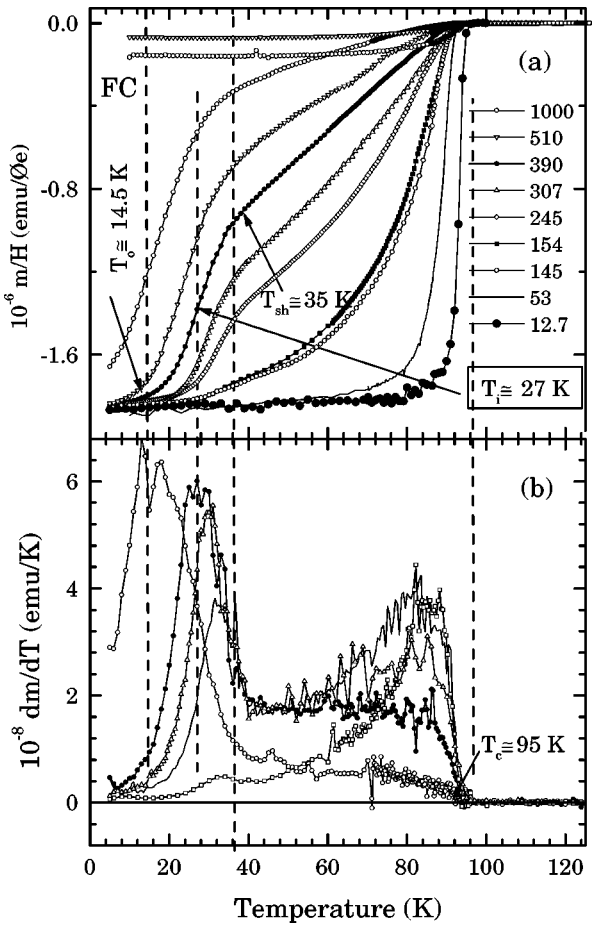

FIG. 4. Zero-field-cooled (ZFC) magnetic moment vs temperature of a $HgBa_2CuO_{4+\delta}$ single crystal for several dc magnetic fields applied parallel to the c axis.

We turn now to the discussion of the ZFC $m(T)$ curves for $H_{dc} \geqslant 1.5$ kOe. Figure 5 shows the ZFC $m(T)$ curves for $H_{dc} \geqslant 1.5$ kOe. Here $-m$ decreases abruptly up to a temperature $T_{sh}(H_{dc})$ and after this point it still decreases but with a much smaller rate. The horizontal, low-temperature part of the shoulder structure is absent because H_{dc} is greater than $H_{c1}(0)$. Although $-m$ seems to decrease up to $T_{c2}(H_{dc})$ without any feature, close examination near the $m = 0$ axis reveals an appreciable change in dm/dT at $T = T_{irr}$ (Fig. 6).

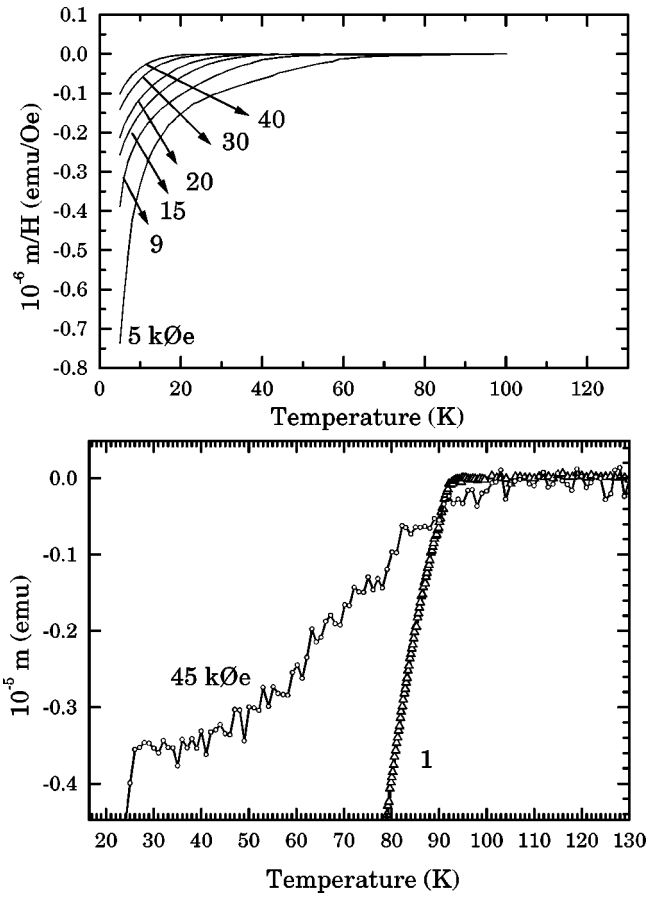

FIG. 5. (a) Zero-field-cooled (ZFC) magnetic moment vs temperature of a $HgBa_2CuO_{4+\delta}$ single crystal for several dc-magnetic fields ($H>1.5$ kOe) applied parallel to the c axis. (b) Rescaled (magnified) plot of the ZFC magnetic moment for $H=1$ and 45 kOe.

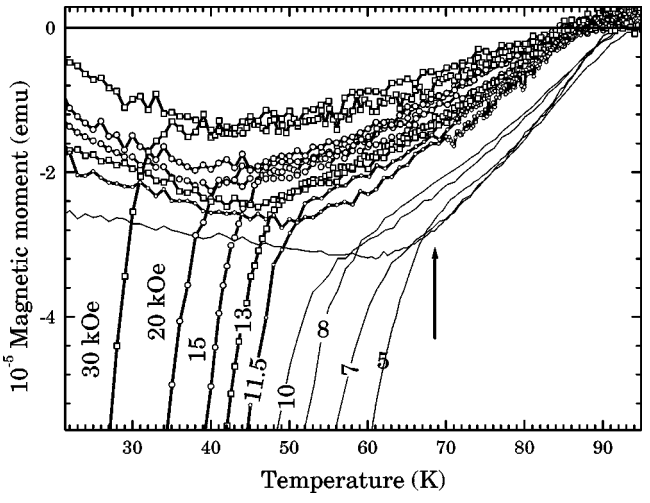

FIG. 6. Rescaled (magnified) plot of the zero-field-cooled (ZFC) and field-cooled (FC) magnetic moment vs temperature variation of a $HgBa_2CuO_{4+\delta}$ single crystal for several dc magnetic fields ($H>1.5$ kOe) applied parallel to the c axis. We define the irreversibility point (H_{irr},T_{irr}) as the point where the $m(T)$ curve changes its slope abruptly. This point coincides with the point where the ZFC and FC branches diverge.

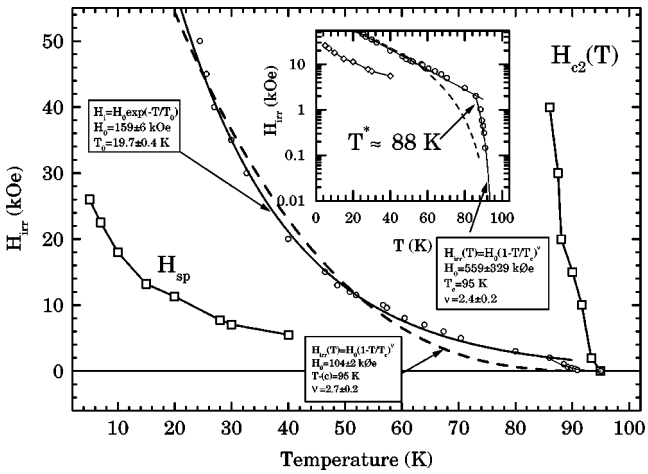

FIG. 7. The irreversibility line of a $HgBa_2CuO_{4+\delta}$ single crystal as a function of temperature for $H\|c$. At $T^*\approx 88$ K, $H_{irr}(T)$ displays an abrupt change in its slope. The solid line represents an $H_{irr}(T)=H_0\exp(-T/T_0)$ fit with parameters estimated by least-squares fitting. The dash line is a power-law fit $[H_{irr}(T)=H_0(1-T/T_c)^{\nu}]$. The inset shows the temperature dependence $H_{irr}(T)$ in a semilog arithmic plot, where an abrupt change in the slope of H_{irr} is clearly seen. Above T^* the experimental points can be fitted by a power law $[H\propto(T-T_c)^{\nu=2.4}]$. The H_{c2} line has been estimated by linear extrapolation of the linear part of $m(T)$ near the T_c.

For $T>T_{irr}$, $m(T)$ is convex up to the T_c region where it becomes concave. Field-cooling measurements at the same field as the ZFC branch reveal that the temperature where the ZFC and FC branches diverge is near T_{irr}. So we define the irreversibility temperature as the point where m changes slope abruptly. Of course the irreversibility line which is defined as the point where the ZFC and FC branches diverge depends on the resolution of the SQUID magnetometer ($\Delta m\approx 2\times 10^{-6}$ emu). The $T_{irr}(H_{dc})$ points represent a low boundary of the irreversibility line. For $H_{dc}\leqslant 5$ kOe the abrupt change in dm/dT is not so pronounced or it disappears and therefore in this regime we define T_{irr} as the point where the ZFC and FC branches diverge.

At high magnetic fields (e.g., 30 kOe) the FC branch of $m(T)$ at low temperature shows a small change from positive to negative slope. This change could originate from the sample holder or from a small amount of paramagnetic material present on the surface of the crystal. We must keep in mind that the signal in this region (for the particular single crystal) is very small, and consequently the paramagnetic impurities at this temperature have a non-negligible contribution to the SQUID signal.

In Fig. 7 we have plotted the points (H_{dc},T_{irr}). This plot is one of the main results of our work. In a semilogarithmic plot we can easily observe at $H^*\approx 2$ kOe (or equivalently at $T^*\approx 88$ K) an abrupt change in the slope of the irreversibility line. The same changes in the slope of the $H_{irr}(T)$ curve have been observed by Wisniewski *et al.*[20] from magnetic measurements in a $HgBa_2Ca_2Cu_3O_{8+\delta}$ single crystal. Probably this point is some crossover or a triclinic point. This behavior has been observed in both $YBa_2Cu_3O_{6.95}$ and $Bi_2Sr_2CaCu_2O_{8+\delta}$compounds. For $T>T^*$ the flux line melts via a first order transition. Below this temperature the solid to liquid transformation is of second order. Alternatively, the

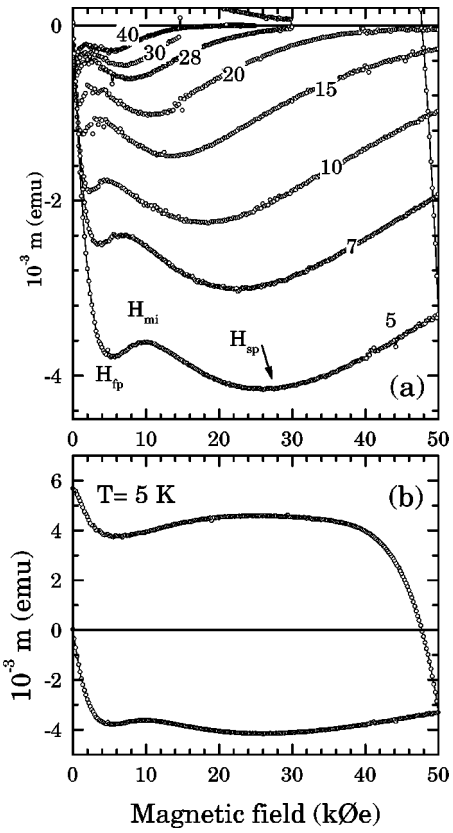

FIG. 8. Virgin magnetization measurements at $5 \leqslant T \leqslant 50$ K of the $HgBa_2CuO_{4+\delta}$ single crystal as a function of the dc-magnetic field H ($H \| c$). The inset shows the ascending and descending branches at $T=5$ K. At $T=5$ K the virgin magnetization starts to deviate from linearity at 500 Oe.

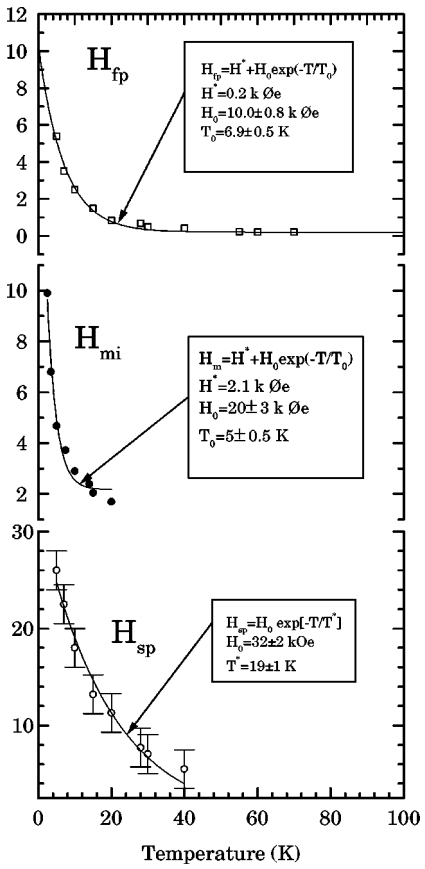

FIG. 9. Temperature dependence of the first peak (H_{fp}), minimum (H_m), and second peak (H_{sp}) fields of the magnetization curve of a $HgBa_2CuO_{4+\delta}$ single crystal for $H \| c$. The solid lines in the plots represent the curves $H_i(T)=H_0^i \exp(-T/T_0^i)$ with parameters which were estimated by least-squares fitting.

(H^*, T^*) point represents a crossover from 3D ($T>T^*$) to 2D behavior of the vortices. For optimally doped $Bi_2Sr_2CaCu_2O_{8+\delta}$, H^* is 260 Oe,[21] while for $YBa_2Cu_3O_{6.95}$ it is 80 kOe.[22] The (H^*, T^*) point moves to highest H and smaller T values as the oxygen content increases and thus changes the anisotropy of the compound. $HgBa_2CuO_{4+\delta}$ displays an anisotropy between those of $YBa_2Cu_3O_{6.95}$ and $Bi_2Sr_2CaCu_2O_{8+\delta}$. Le Bras *et al.*[23] and Hofer *et al.*[24] estimated the anisotropy parameter for $HgBa_2CuO_{4+\delta}$ to be $\varepsilon^{-1} \approx 30$, while for YBCO, $\varepsilon^{-1} \approx 5$, and for BSCCO, $\varepsilon^{-1} \approx 50$. The intermediate value of the anisotropy parameter for $HgBa_2CuO_{4+\delta}$ can explain the observed behavior. Below T^* the irreversibility field increases exponentially with temperature. The experimental points can be described as $H_{irr} = H_0 \exp(-T/T_0)$. Least-squares fitting gives $H_0 = 159 \pm 6$ kOe and $T_0 = 19.7 \pm 0.4$ K. An effort to fit the H_{irr} with a power law [$H_{irr} \propto (1-T/T_c)^{\nu}$ for $T<T^*$] was unsuccessful (see dashed line in Fig. 7). For $T>T^*$ the irreversibility line can be roughly approximated with a power law with exponent $\nu \approx 2.4$.

Finally we present hysteresis loop measurements. The magnetic hysteresis loops were measured at low temperatures ($5 \leqslant T \leqslant 40$ K) and are shown in Fig. 8. The virgin (ascending magnetic field branch) branch shows a peak at low fields (which we call the first peak and denote as H_{fp}), followed by a decrease in m which means penetration of the vortices. As the magnetic field increases $-m$ reaches a local minimum at H_m. After this point $-m$ increases irregularly with increasing field up to the magnetic field H_{sp} and finally for $H>H_{sp}$ it decreases towards the equilibrium magnetic moment. The (H_{sh}, T_{sh}) point as in the case of lower fields denotes the state of complete flux penetration in the sample. These values coincide with the H_{fp} values. That is, point (H_{sh}, T_{sh}) corresponds to the (H_{fp}, T) point. Considering the crystal as a thick disk with diameter $2a=200$ μm and thickness $2b=50$ μm and using the formula for full penetration of the magnetic field of Forkl,[25] $H_{fp} = (4\pi/c) J_c b \ln[(a/b)+(1+a^2/b^2)^{1/2}]$ we can calculate J_c from H_{fp}. For example, $H_{fp} \simeq 5$ kOe at 5 K which gives $J_c \simeq 7.6 \times 10^5$ A/cm^2. Upon decreasing the magnetic field the magnetic moment approximately has the opposite value of that of the ascending branch. In other words, the hysteresis loop is symmetric about the $m=0$ axis (neglecting contributions from the equilibrium magnetization). The symmetric hysteresis loop is in agreement with Bean's model, which predicts a symmetric hysteresis loop. Early magnetic hysteresis loops $m(H,T)$ in polycrystalline $HgBa_2CuO_{4+\delta}$ samples[26–28] have shown a considerable asymmetry regarding the field-increasing and field-decreasing branches. Furthermore, the magnetization in the field-decreasing branch is very small, suggesting that surface pinning dominates in this material. However, for our single crystal the loops are symmetric, and so we can exclude, especially at low T and high

fields, an interpretation based on the surface barrier effect.

Figure 9 shows the variation of H_{fp}, H_m, and H_{sp} with temperature. We modeled all three curves as exponential functions of temperature e.g., $H_i = H_0^i \exp(-T/T_0^i)$. The characteristic parameters for the second peak were estimated to be $H_0^{sp} = 32 \pm 2$ kOe, and $T_0^{sp} = 19 \pm 1$ K. For the first peak, $H_0^{fp} = 10 \pm 1$ kOe and $T_0^{fp} = 6.9 \pm 0.5$ K, and for the minimum, $H_0^m =$ 20 kOe, and $T_0^m = 5 \pm 1$ K. The so-called fishtail effect is also present in the well-studied compounds $YBa_2Cu_3O_7$ and $Bi_2Sr_2CaCu_2O_{8+\delta}$. The mechanism that gives rise to the fishtail effect remains controversial. In the past, it was attributed to sample inhomogeneities, to a 3D to 2D vortex lattice transition or to a crossover between bulk pinning and surface barriers. In the case of $Bi_2Sr_2CaCu_2O_{8+\delta}$ the peak is sharp and is observed only for a narrow temperature range ($20 < T < 50$). In $YBa_2Cu_3O_{6.95}$ Abulafia *et al.*[29] attributed the fishtail effect to a crossover in flux dynamics from elastic to plastic creep. Deligiannis *et al.*[22] confirmed and clarified even further the situation. A new interpretation of this peak is that it comes from a second-order thermodynamic vortex phase transition.[30–32] It was proposed that the peak line separates two distinct solid phases. A weakly disordered quasilattice is associated with the Bragg glass phase (for low fields below the second peak) and a highly disordered entangled solid (or vortex glass or a liquid) at higher fields.

VI. CONCLUSIONS

In summary, we report on the single-crystal structure and the magnetic properties of $HgBa_2CuO_{4+\delta}$ with $T_c = 95$ K. The main points of the crystal structure are the cell constants [$a = 3.888(1)$ Å, $c = 9.538(2)$ Å], the anomalously large anisotropic displacement thermal factors U_{11} and U_{33} for Hg, and the interstitial oxygen content which is estimated to be $\delta \simeq 0.08(4)$. Magnetic hysteresis loops at $T < 50$ K show the fishtail effect. All the features of the hysteresis loops (H_{fp}, H_m, H_{sp}) decrease exponentially with temperature. From the hysteresis loops and the ZFC-FC magnetization measurements we estimated the irreversibility field (or melting field) as a function of temperature. The variation with temperature ($20 \leqslant T \leqslant 88$ K) is exponential [$H_i = H_0 \exp(-T/T_0)$, $H_0 = 159$ kOe, $T_0 = 19.7$ K], and for $T > T^* = 88$ K the irreversibility line changes slope, revealing the existence of a crossover or tricritical point in the phase diagram.

[1] A. F. Maiorova *et al.*, Thermochim. Acta **269**, 101 (1995).
[2] J. Karpinski, H. Schwer, I. Mangelschots, K. Conder, A. Morawski, T. Lada, and A. Parzewin, Physica C **234**, 10 (1994).
[3] D. Pelloquin, A. Maignan, A. Gueston, V. Hardy, and B. Raveau, Physica C **265**, 5 (1996).
[4] A. Bertinotti, V. Viallet, D. Colson, J.-F. Marucco, J. Hammann, G. Le Bras, and A. Forget, Physica C **268**, 257 (1996).
[5] P. Bordet, F. Duc, S. LeFloch, J. J. Capponi, E. Alexandre, M. Rosa-Nunes, S. Putilin, and E. V. Antipov, Physica C **271**, 189 (1996).
[6] D. Pelloquin, V. Hardy, A. Maignan, and B. Raveau, Physica C **273**, 205 (1997).
[7] M. Pissas, B. Billon, M. Charalambous, J. Chaussy, S. LeFloch, P. Bordet, and J. J. Caponi, Supercond. Sci. Technol. **10**, 598 (1997).
[8] G. Blatter, M. V. Feigel'man, V. B. Geshkenbein, A. I. Larkin, and V. M. Vinokur, Rev. Mod. Phys. **66**, 1125 (1994).
[9] B. Billon, M. Charalambous, O. Riou, J. Chaussy, and D. Pelloquin, Phys. Rev. B **56**, 10 824 (1997).
[10] S. N. Putilin, E. V. Antipov, O. Chmaissem, and M. Marezio, Nature (London) **362**, 226 (1993).
[11] Q. Huang, J. W. Lynn, Q. Xiong, and C. W. Chu, Phys. Rev. B **52**, 462 (1995).
[12] J. L. Wagner *et al.*, Physica C **210**, 447 (1993).
[13] A. Asab, A. R. Armstrong, I. Gameson, and P. P. Edwards, Physica C **255**, 180 (1995).
[14] J. R. Clem and Z. Hao, Phys. Rev. B **48**, 13 774 (1993).
[15] L. Krusin-Elbaum, A. P. Malozemoff, Y. Yeshurun, D. C. Cronemeyer, and F. Holtzberg, Phys. Rev. B **39**, 2936 (1989).
[16] L. Krusin-Elbaum, A. P. Malozemoff, D. C. Cronemeyer, F. Holtzberg, J. R. Clem, and Z. Hao, J. Appl. Phys. **67**, 4670 (1990).
[17] F. De la Cruz, H. Pastoriza, and A. Arribere, *Studies in High Temperature Superconductors* (Nova Science, Commack, NY, 1994), Vol. 14, p. 307.
[18] M. F. Goffman, J. A. Herbsommer, F. de la Cruz, T. W. Li, and P. H. Kes, Phys. Rev. B **57**, 3663 (1998).
[19] M. Nideröst, A. Suter, P. Visani, A. C. Mota, and G. Blatter, Phys. Rev. B **53**, 9286 (1996).
[20] A. Wisniewski, R. Szymczak, M. Baran, R. Puzniak, J. Karpinski, R. Molinski, H. Schwer, K. Conder, and I. Meijer, Czech. J. Phys. **46**, S31 649 (1996).
[21] B. Khaykovich, M. Konczykowski, E. Zeldov, R. A. Doyle, D. Majer, P. H. Kes, and T. W. Li, Phys. Rev. B **56**, R517 (1997).
[22] K. Deligiannis, P. A. J. de Groot, M. Oussena, S. Pinfold, R. Langan, R. Gagnon, and L. Taillefer, Phys. Rev. Lett. **79**, 2121 (1997).
[23] G. Le Bras, L. Fruchter, V. Vulcanescu, V. Viallet, A. Bertinotti, A. Forget, J. Hammann, J.-F. Marucco, and D. Colson, Physica C **271**, 205 (1996).
[24] J. Hofer, J. Karpinski, M. Willemin, G. I. Meijer, E. M. Kopnin, R. Molinski, H. Schwer, C. Rossel, and H. Keller (unpublished).
[25] A. Forkl, Phys. Scr. **49**, 148 (1993).
[26] Y. R. Sun, J. R. Thompson, H. R. Kerchner, D. K. Christen, M. Paranthaman, and J. Brynestad, Phys. Rev. B **50**, 3330 (1994).
[27] J. A. Lewis, V. M. Vinokur, J. Wagner, and D. Hinks, Phys. Rev. B **52**, R3852 (1995).
[28] J. R. Thompson, H. R. Khan, and K. J. Song, Physica C **272**, 271 (1996).
[29] Y. Abulafia, A. Shaulov, Y. Wolfus, R. Prozorov, L. Burlachkov, Y. Yeshurun, D. Majer, E. Zeldov, H. Wühl, V. B. Geshkenbein, and V. M. Vinokur, Phys. Rev. Lett. **77**, 1596 (1996).
[30] T. Giamarchi and P. Le Doussal, Phys. Rev. B **52**, 1242 (1995).
[31] T. Giamarchi and P. Le Doussal, Phys. Rev. B **55**, 6577 (1997).
[32] A. E. Koshelev and V. M. Vinokur, Phys. Rev. B **57**, 8026 (1998).